*R*esearch in
*A*stronomy and
*A*strophysics

Photometric analysis and evolutionary stages of the contact binary V2790 Ori

Wichean Kriwattanawong[1,2] and Kriangsak Kriwattanawong[3]

[1] Department of Physics and Materials Science, Faculty of Science, Chiang Mai University, Chiang Mai, 50200, Thailand; *wichean.k@cmu.ac.th*

[2] Research Center in Physics and Astronomy, Faculty of Science, Chiang Mai University, Chiang Mai, 50200, Thailand

[3] Department of Chemical Engineering, Faculty of Engineering, King Mongkut's Institute of Technology Ladkrabang, Bangkok 10520, Thailand

Abstract A photometric analysis and evolutionary stages of the contact binary V2790 Ori are presented. The BVR_C observations were carried out at the Thai National Observatory. The photometric light curves were fitted to provide fundamental parameters, required to examine evolutionary stages of the binary. The results indicate that V2790 Ori is a W-type contact system with a mass ratio of $q = 2.932$. The orbital period increase is found at a rate of $\mathrm{d}P/\mathrm{d}t = 1.03 \times 10^{-7}\,\mathrm{d\,yr^{-1}}$. This implies that a rate of mass transfer from the secondary component to the primary one is $\mathrm{d}m_2/\mathrm{d}t = 6.31 \times 10^{-8}\,M_\odot\,\mathrm{yr^{-1}}$. Furthermore, we find that from the detached phase to the contact phase, the amount of mass that the evolved secondary component has lost is $1.188 \pm 0.110\,M_\odot$, i.e., mass lost by the system is $0.789 \pm 0.073\,M_\odot$ and mass transfer to the primary is $0.399 \pm 0.037\,M_\odot$. Since the time of the first overflow, the angular momentum loss is found to be 72.2% of J_FOF, causing the orbit and Roche surface to shrink until the present time.

Key words: stars: binaries: close — stars: binaries: eclipsing — stars: individual: V2790 Ori

1 INTRODUCTION

Contact binaries are believed to have been formed from detached systems by evolutionary expansion of the components or angular momentum loss (AML) due to magnetic breaking (e.g., Vilhu 1981; Rucinski 1986; Jiang et al. 2014). Demircan et al. (2006) provided evidence of decreasing rates in angular momentum, systematic mass and orbital period from a sample of 114 detached systems, derived from their kinematics. However, the evolution is controlled not only by the AML but also by mass loss and mass transfer between the components (e.g., Yakut & Eggleton 2005; Eker et al. 2008). The evolution is driven by a slow expansion of the progenitor of the secondary component (the evolved component near or after the terminal age main sequence), followed by mass transfer to the other component, accompanied by AML due to stellar winds and mass loss. The components of close detached binaries approach each other to form contact binaries. The continuous AML and mass loss can bring the components closer together, yielding a smaller orbit and shrinking the Roche surface

(e.g., Vilhu 1981; Iben & Tutukov 1984; Tutukov et al. 2004; Gazeas & Stępień 2008; Stępień & Gazeas 2012).

V2790 Ori [R.A.(J2000.0)=$06^\mathrm{h}15^\mathrm{m}31.40^\mathrm{s}$, Dec.(J2000.0)= $+19°35'\,22.1''$] is a contact binary, found in the Northern Sky Variability Survey (NSVS). Its orbital period was firstly reported by Otero et al. (2004) to be 0.287842 d with a primary minimum at HJD 2451521.695. Two years later, Ammons et al. (2006) contributed the effective temperature of V2790 Ori to be 5643 K. Furthermore, two recent values of the effective temperature of 5713 K and 5576 K were cataloged by McDonald et al. (2017) and Oelkers et al. (2018), respectively. The average value was calculated to be about 5644 K.

This work presents a photometric analysis and evolutionary stages of the contact binary V2790 Ori. The BVR_C photometric observations are described in Section 2. Section 3 presents an analysis of a period change. Section 4 explains the results of the light curve fit. Section 5 describes the evolutionary stages, including mass

change throughout its evolution from the detached phase to the contact phase and orbital evolution by AML from the time of the first overflow (FOF) to the present time. Finally, the main results are summarized in Section 6.

2 OBSERVATIONS

V2790 Ori was observed with the 0.5 m reflecting telescope, operated by Thai National Observatory, Chiang Mai, during three nights in 2015 (January 21–23). An Andor iKon-L-936 CCD camera was equipped on the telescope. Total integration times were 120 s for B band and 60 s for V and R_C bands. We obtained a total of 699 individual observations for the three filter bands. The BVR_C differential magnitudes of the binary were measured using TYC 1322-1399-1 [R.A.(J2000.0) $= 06^h15^m19.52^s$, Dec.(J2000.0) $= +19°37' 07.6''$] and TYC 1322–1411–1 [R.A.(J2000.0) $= 06^h15^m05.39^s$, Dec.(J2000.0) $= +19°40' 43.3''$] as comparison and check stars, respectively. The observed magnitudes cover light curves with five minimum light times as shown in Table 1. The tricolor light curves vary about 0.64, 0.59 and 0.56 mag, for the B, V and R_C bands, respectively. Max II is found to be slightly brighter than Max I.

3 PERIOD ANALYSIS

The first estimate of orbital period for the contact binary V2790 Ori was provided by Otero et al. (2004). Until the present day, 36 eclipse timings, including this work, are available as listed in Table 1. Since the first two times are too far from the others, the last 34 times were used to calculate the orbital period as shown in Equation (1). The revised period is found to be 0.2878418 d.

$$\text{Min.I} = \text{HJD } 2457043.9349(\pm0.0002) \\ + 0.2878418(\pm0.0000001) \times E \,. \tag{1}$$

$$(O - C) = -0.00005(\pm0.00021) \\ + 1.67(\pm2.45) \times 10^{-7}E \\ + 4.06(\pm5.63) \times 10^{-11}E^2 \,. \tag{2}$$

With the above ephemeris, a least squares method was used to fit the $(O - C)$ residuals as shown in Equation (2). The $(O - C)$ fit yields an upward quadratic curve as displayed in Figure 1. This can be interpreted as the orbital period increase at a rate of $dP/dt = 1.03\times10^{-7}\,\text{d yr}^{-1}$.

4 LIGHT CURVE FIT

An analysis of the tricolor light curves for V2790 Ori was done by using the 2013 version of the Wilson-Devinney

Table 1 Times of Minimum Light for V2790 Ori

HJD (1)	Min (2)	Ref. (3)	Epoch (4)	$(O - C)$ (5)
2451521.6950	I	[1]		
2453327.7560	II	[2]		
2455520.8205	II	[3]	–5291.5	0.0005
2455532.9103	II	[2]	–5249.5	0.0009
2455604.2950	II	[4]	–5001.5	0.0009
2455632.3597	I	[4]	–4904.0	0.0010
2455644.3050	II	[4]	–4862.5	0.0009
2455896.8827	I	[5]	–3985.0	–0.0026
2455902.7850	II	[6]	–3964.5	–0.0011
2455959.3466	I	[7]	–3768.0	–0.0004
2456288.0610	I	[8]	–2626.0	–0.0013
2456288.2045	II	[8]	–2625.5	–0.0018
2456623.1092	I	[9]	–1462.0	–0.0010
2456623.2547	II	[9]	–1461.5	0.0006
2457041.6326	I	[10]	–8.0	0.0004
2457041.7767	II	[10]	–7.5	0.0006
2457042.6403	II	[10]	–4.5	0.0007
2457042.7836	I	[10]	–4.0	0.0000
2457044.0792	II	[11]	0.5	0.0004
2457045.0865	I	[11]	4.0	0.0002
2457045.2306	II	[11]	4.5	0.0004
2457046.0942	II	[11]	7.5	0.0005
2457046.2377	I	[11]	8.0	0.0000
2457048.6848	II	[10]	16.5	0.0005
2457048.8286	I	[10]	17.0	0.0004
2457049.6919	I	[10]	20.0	0.0001
2457049.8362	II	[10]	20.5	0.0005
2457050.6995	II	[10]	23.5	0.0003
2457050.8432	I	[10]	24.0	0.0001
2457064.3746	I	[12]	71.0	0.0029
2457345.7361	II	[10]	1048.5	–0.0010
2457345.8798	I	[10]	1049.0	–0.0012
2457346.7434	I	[10]	1052.0	–0.0011
2457346.8876	II	[10]	1052.5	–0.0008
2457384.0202	II	[13]	1181.5	0.0002
2457384.1636	I	[13]	1182.0	–0.0003

Notes: Column (1): HJD at light minimum. Col. (2): types of minimum. Col. (3): references for the sources are as follows: [1] Otero et al. (2004); [2] Diethelm (2011); [3] Nelson (2011); [4] Nagai (2012); [5] Diethelm (2012); [6] Nelson (2012); [7] Hubscher (2013); [8] Nagai (2013); [9] Nagai (2014); [10] Michaels (2016); [11] This study; [12] Juryšek et al. (2017); [13] Nagai (2016). Col. (4): epoch. Col. (5): $(O - C)$.

(W-D) code (Wilson & Devinney 1971; Wilson 1979, 2012; Wilson et al. 2010). According to three available published values of effective temperature, as mentioned in Section 1, the average value of 5644 K was assigned to fix the temperature of star 2, T_2. The adjustable parameters (the mass ratio, q; the effective temperature of star 1, T_1; the surface potential of the components, $\Omega_1 = \Omega_2$; the orbital inclination, i; and the monochromatic luminosities of star 1, L_1) were applied to the W-D fit. A spot was added on star 1. A q-search procedure was iterated over a wide range of mass ratio to minimize sum of squared residuals $\Sigma W(O - C)^2$. A good fit is found at about $q \sim 3$ as illustrated in Figure 2. With more precise
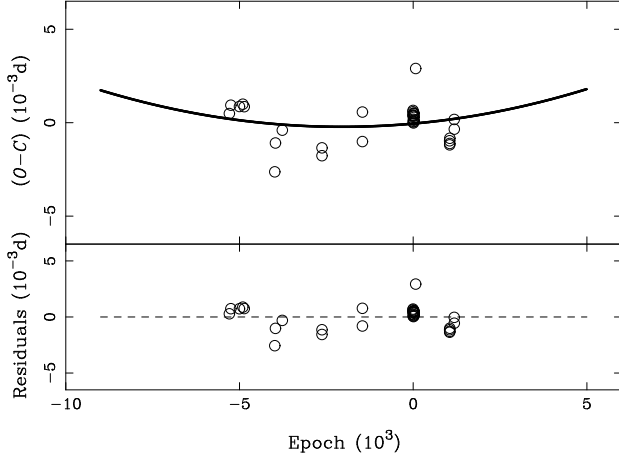
Fig. 1 $(O - C)$ curve (*upper*) and the corresponding residuals (*lower*) for V2790 Ori.

iterations, the minimum value of $\Sigma W(O-C)^2$ is obtained at $q = 2.932\pm0.002$. The results show that V2790 Ori is a W-type contact binary. Contact configuration of the system is not very deep with a fill-out factor of 20.89±1.03%. A total eclipse is confirmed by the orbital inclination of 85.1°. The derived temperature ratio of T_2/T_1 is 0.964. A cool spot on star 1 can explain the asymmetric light maxima, well-known as the O'Connell effect. This effect was also similarly found to be evidence of star-spot activities on one component or both components in many W-type contact systems such as V789 Her (Li et al. 2018), V474 Cam (Guo et al. 2018), RW Dor (Sarotsakulchai et al. 2019) and TY UMa (Li et al. 2015). The fitted light curves are depicted in Figure 3. The main parameters are listed in Table 2, and compared with those from a previous work (Michaels 2016). The mass ratio and fill-out factor in this study are not very different from those in the previous work. The other parameters are nearly the same, except the effective temperatures, due to the value of T_2 being fixed with different assumptions and source data. However, the temperature ratio is still the same.

5 EVOLUTIONARY STAGES

5.1 Mass Change

To understand the evolutionary status of this contact binary, we first calculated masses of both components using correlations between mass, orbital period and mass ratio (Gazeas 2009). We find that $M_1 = 0.348\pm0.038\,M_\odot$ and $M_2 = 1.020\pm0.112\,M_\odot$ for the secondary and primary components, respectively. According to the orbital period increase with a rate of $dP/dt = 1.03\times10^{-7}\,\mathrm{d\,yr^{-1}}$,

Table 2 Photometric Parameters for V2790 Ori

| Parameters	Michaels (2016)	This study
q	3.157($\pm$0.008)	2.932($\pm$0.002)
T_1(K)	5620($\pm$3)	5856($\pm$9)
T_2(K)	5471	5644
i (°)	84.15($\pm$0.20)	85.1($\pm$0.2)
$\Omega_1 = \Omega_2$	6.732($\pm$0.010)	6.397($\pm$0.007)
$L_{1B}/(L_{1B} + L_{2B})$	-	0.3229($\pm$0.0010)
$L_{1V}/(L_{1V} + L_{2V})$	-	0.3106($\pm$0.0007)
$L_{1R_c}/(L_{1R} + L_{2R_c})$	-	0.3048($\pm$0.0006)
$L_{1g'}/(L_{1g'} + L_{2g'})$	0.2966($\pm$0.0007)	-
$L_{1r'}/(L_{1r'} + L_{2r'})$	0.2867($\pm$0.0005)	-
$L_{1i'}/(L_{1i'} + L_{2i'})$	0.2830($\pm$0.0005)	-
r_1 (pole)	-	0.2798($\pm$0.0009)
r_1 (side)	-	0.2929($\pm$0.0011)
r_1 (back)	-	0.3330($\pm$0.0021)
r_2 (pole)	-	0.4544($\pm$0.0007)
r_2 (side)	-	0.4891($\pm$0.0010)
r_2 (back)	-	0.5182($\pm$0.0013)
f (%)	15	20.89($\pm$1.03)
$\Sigma W(O - C)^2$	0.0056	0.0035
Spot 1 on star 1	Hot spot	Cool spot
Spot Colatitude (°)	105($\pm$5)	37($\pm$3)
Spot Longitude (°)	10($\pm$3)	264($\pm$4)
Spot Radius (°)	14($\pm$4)	26($\pm$2)
Temperature Factor	1.16($\pm$0.05)	0.90($\pm$0.03)
Spot 2 on star 2	Cool spot	
Spot Colatitude (°)	78($\pm$4)	-
Spot Longitude (°)	2($\pm$1)	-
Spot Radius (°)	12($\pm$4)	-
Temperature Factor	0.90($\pm$0.05)	-
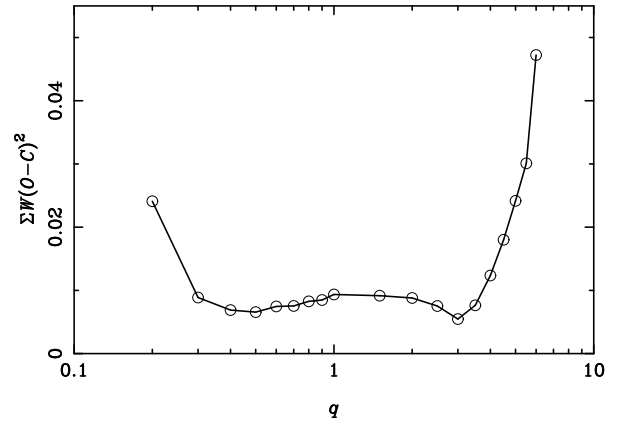
Fig. 2 q-search values for V2790 Ori.

described in Section 3, a mass transfer rate from the less massive hotter component to the other one can be estimated using Equation (3) (Singh & Chaubey 1986; Pribulla 1998). The mass transfer rate is obtained to be $dM_2/dt = 6.31\times10^{-8}\,M_\odot\,\mathrm{yr^{-1}}$.

$$\frac{\dot{P}}{P} = 3\left(\frac{M_2}{M_1} - 1\right)\frac{\dot{M_2}}{M_2}. \tag{3}$$

Table 3 W-type Contact Systems with Increasing Orbital Period

Contact Systems	P (d)	q	i (°)	f (%)	T_1(K)	T_2(K)	dP/dt (d yr^{-1})	Ref.*
AA UMa	0.4681266	1.819	80.3	14.8	5965	5929	4.70×10^{-8}	[1]
AB And	0.3318911	1.786	83.2	25.2	5888	5495	1.46×10^{-7}	[2]
AH Vir	0.4075243	3.317	86.5	24.0	5671	5300	2.19×10^{-7}	[3]
FI Boo	0.3899980	2.680	38.1	50.2	5746	5420	1.65×10^{-7}	[4]
TX Cnc	0.3828832	2.220	62.1	24.8	6537	6250	3.70×10^{-8}	[5]
TY Uma	0.3545481	2.523	84.9	13.4	6250	6229	5.18×10^{-7}	[6]
UX Eri	0.4452823	2.681	76.9	14.0	6100	6046	7.70×10^{-8}	[7]
V728 Her	0.4712901	5.607	69.2	71.0	6787	6622	3.79×10^{-7}	[8]
V1191 Cyg	0.3133888	9.360	80.8	57.9	6375	6215	3.13×10^{-6}	[9]
V2790 Ori	0.2878418	2.932	85.1	21.6	5856	5644	1.03×10^{-7}	[10]

Notes: * References for the sources are as follows: [1] Lee et al. (2011); [2] Li et al. (2014); [3] Chen et al. (2015); [4] Christopoulou & Papageorgiou (2013); [5] Zhang et al. (2009); [6] Li et al. (2015); [7] Qian et al. (2007); [8] Yu et al. (2016); [9] Ostadnezhad et al. (2014); [10] This study.
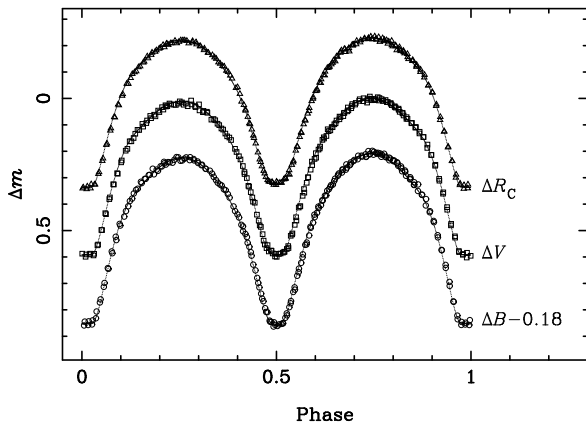

Fig. 3 Observed light curves in B (*circles*), V (*squares*) and R_C (*triangles*) filter bands and theoretical light curves (*solid lines*) versus orbital phase of V2790 Ori.

Some W-type contact systems with increasing orbital period were collected to compare the value of dP/dt as listed in Table 3. The period increasing rate for V2790 Ori is found to be a typical value with respect to other W-type systems.

The photometric parameters in Section 4 are used to calculate radii and luminosities of the components, and the semimajor axis of the orbit, which are derived to be $R_1 = 0.613\pm0.018\,R_\odot$, $R_2 = 0.991\pm0.029\,R_\odot$, $L_1 = 0.396\pm0.016\,L_\odot$, $L_2 = 0.892\pm0.036\,L_\odot$ and $a = 2.036\pm0.059\,R_\odot$, respectively. Masses of both components in the study are slightly greater than values in Michaels (2016)'s work because of the different method of calculations. In this study, we applied the three-dimensional correlations of physical parameters provided by Gazeas (2009), while Michaels (2016) employed the mass-period relation supplied by Qian (2003). Accordingly, our values of R_1, R_2, L_1, L_2 and a are
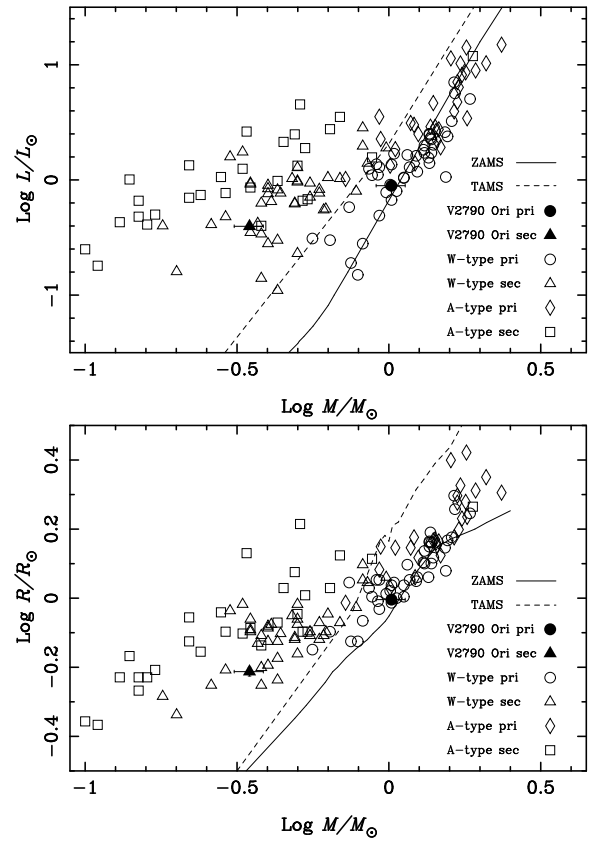

Fig. 4 Both components of V2790 Ori on the $\log M - \log L$ (*upper*) and $\log M - \log R$ (*lower*) diagrams: the primary more massive (*filled dot*) and the secondary less massive (*filled triangle*) components. The sample of contact binaries, collected from the work of Yakut & Eggleton (2005), is plotted for comparison. The *solid* and *dashed lines* are for ZAMS and TAMS, respectively, constructed by the Hurley et al. (2002) binary star evolution code for solar metallicity.

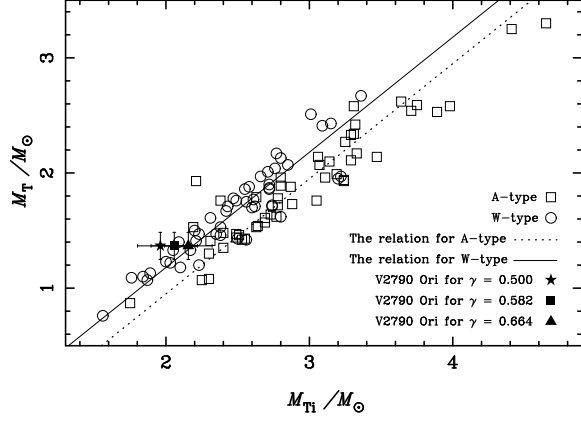slightly greater than values in the previous work as listed in Table 4.

Fig. 5 Total initial mass of V2790 Ori for the three cases of γ on the M_T–M_{Ti} diagram. The *dotted* and *solid lines* are the M_T–M_{Ti} relations, fitted by Yıldız (2014) using a sample of 51 A-type (*open squares*) and 49 W-type (*open circles*) contact systems, respectively. V2790 Ori with the value of $\gamma = 0.664$ (*filled triangle*) is located closer to the relation than the cases of $\gamma = 0.582$ (*filled square*) and $\gamma = 0.500$ (*filled star*).

The mass–luminosity and mass–radius diagrams in Figure 4 are plotted to compare evolutionary status for both components of V2790 Ori with the zero age main sequence (ZAMS) and terminal age main sequence (TAMS), constructed by the Hurley et al. (2002) binary star evolution code. The other well-known contact systems were obtained from the catalog of Yakut & Eggleton (2005). It is found that the primary component of V2790 Ori is located near the ZAMS, similar to the primary stars of other W-type systems, implying that its evolutionary stage remains in the main sequence phase, while the secondary component of V2790 Ori lies above the TAMS, indicating that the secondary component has evolved to be oversized and overluminous. We calculated the mean densities of the components using the equations taken from Mochnacki (1981)

$$\overline{\rho}_1 = \frac{0.079}{V_1(1+q)P^2}, \tag{4}$$

$$\overline{\rho}_2 = \frac{0.079q}{V_2(1+q)P^2}, \tag{5}$$

where the relative volumes of the components V_1 and V_2 are normalized to the semimajor axis, q is the mass ratio and P is the orbital period. We obtained $\overline{\rho}_1 = 2.121\pm0.259\,\mathrm{g\,cm^{-3}}$ and $\overline{\rho}_2 = 1.474\pm0.179\,\mathrm{g\,cm^{-3}}$, which are quite close to the values in Michaels (2016)'s work. The mean density of the secondary component, $\overline{\rho}_1$, is less than the theoretical value of the ZAMS star, confirming that the component has evolved away from the ZAMS to become oversized, while the mean density of the solar-mass primary star, $\overline{\rho}_2$, is nearly the same value as the

Table 4 Absolute Parameters for V2790 Ori

Parameters	Michaels (2016)	This study
M_1 ($M_\odot$)	0.30	0.348±0.038
M_2 ($M_\odot$)	0.96	1.020±0.112
R_1 ($R_\odot$)	0.58	0.613±0.018
R_2 ($R_\odot$)	0.97	0.991±0.029
L_1 ($L_\odot$)	0.28	0.396±0.016
L_2 ($L_\odot$)	0.68	0.892±0.036
a ($R_\odot$)	1.98	2.036±0.059
ρ_1 ($\mathrm{g\,cm^{-3}}$)	2.17	2.121±0.259
ρ_2 ($\mathrm{g\,cm^{-3}}$)	1.46	1.474±0.179
$\log g_1$ ($\mathrm{cm\,s^{-2}}$)	4.39	4.406±0.051
$\log g_2$ ($\mathrm{cm\,s^{-2}}$)	4.44	4.456±0.051

Table 5 Mass Parameters Corresponding to the Three Cases of γ for V2790 Ori

Mass parameters	Values	
M_S ($M_\odot$)	0.348(±0.038)	
M_{Si} ($M_\odot$)	1.535(±0.148)	
ΔM ($M_\odot$)	1.188(±0.110)	
M_P ($M_\odot$)	1.020(±0.112)	

	Values for three cases of γ		
γ	0.500	0.582	0.664
M_{Pi} ($M_\odot$)	0.426(±0.057)	0.523(±0.066)	0.620(±0.075)
M_{Ti} ($M_\odot$)	1.961(±0.159)	2.058(±0.162)	2.156(±0.166)
M_{lost} ($M_\odot$)	0.594(±0.055)	0.691(±0.064)	0.789(±0.073)
$M_{transfer}$ ($M_\odot$)	0.594(±0.055)	0.496(±0.046)	0.399(±0.037)

Sun, meaning that the primary component is still a main sequence star.

With the assumption that mass transfer starts, when the secondary (initially more massive) component has evolved to be near or after the TAMS, the initial masses of both components are computed from Equations (6)–(8) (Yildiz & Doğan 2013):

$$M_{Si} = M_S + \Delta M, \tag{6}$$

$$M_{Pi} = M_P - (\Delta M - M_{lost}) = M_P - \Delta M(1-\gamma), \tag{7}$$

$$\Delta M = 2.50\left[(L_S/1.49)^{1/4.216} - M_S - 0.07\right]^{0.64}, \tag{8}$$

where M_{Si} and M_{Pi} are the initial masses, and M_S and M_P are the current masses of the secondary and primary stars, respectively. ΔM is the total mass lost by the secondary, M_{lost} is the mass lost by the binary and γ is the ratio of M_{lost} to ΔM. L_S is the luminosity of the secondary star. The derived value for the initial mass of the secondary star is $1.535\pm0.148\,M_\odot$ and the mass decrease of the secondary is $\Delta M = 1.188\pm0.110\,M_\odot$. However, for W-type contact systems, the value of the fitting parameter γ, given by Yildiz & Doğan (2013), must be in the range of $0.500 < \gamma < 0.664$. Consequently, the corresponding initial mass of the primary star must be a value between 0.426 and $0.620\,M_\odot$, depending on the value of γ.

The precise value of γ needs to be assigned in Equation (7). We applied the minimum, average and maximum values for γ of 0.500, 0.582 and 0.664 respectively for three cases to estimate some possible values of the initial mass of the primary star and total initial mass of the binary. The values of mass lost by the system and mass transfer between the components were finally obtained. The possible mass parameters for the three cases are listed in Table 5. As shown in Figure 5, the total initial mass of V2790 Ori for the case of $\gamma = 0.664$ lies closer to the relation between total present mass (M_T) and total initial mass (M_Ti) for W-type (Yıldız 2014) than the other cases. Thus, the appropriate value of γ for V2790 Ori should be 0.664. The initial mass of the primary component is obtained to be $0.620 \pm 0.075\,M_\odot$. From the detached phase until the present time, some $0.789 \pm 0.073\,M_\odot$ of mass has been lost from the system, while there could be a mass transfer of $0.399 \pm 0.037\,M_\odot$ from the secondary component to the primary component, after the time of FOF.

5.2 Orbital and Angular Momentum Change

In general, the orbital angular momentum can be calculated by using the following well known equation

$$J_\mathrm{o} = \frac{q}{(1+q)^2} \sqrt[3]{\frac{G^2}{2\pi} M_\mathrm{T}^5 P}, \qquad (9)$$

where J_o is the orbital angular momentum, q is the mass ratio, M_T is the total mass of the binary and P is the orbital period. The value of the present angular momentum of the binary is computed to be $\log J_\mathrm{o} = 51.42 \pm 0.06$ cgs. Figure 6 shows a diagram of the orbital angular momentum versus total mass of contact and detached binaries, separated by the quadratic border line (Eker et al. 2006). The sample of detached systems was collected from the catalogs of Eker et al. (2006), Yildiz & Doğan (2013) and Lee (2015). The sample of contact systems was obtained from the works of Eker et al. (2006) and Ibanoğlu et al. (2006). Location of the binary V2790 Ori at the present time (filled triangle) is found to be below the border line, meaning that the present angular momentum of the binary is less than all detached systems with the same mass. This is consistent with angular momentum and/or mass loss in the past during the detached phase causing the binary to evolve into the contact phase.

During the formation of the contact binary V2790 Ori, the AML must continue from detached to semi-detached and contact phases. The orbital period and semimajor axis decrease lead to the components being close together. The
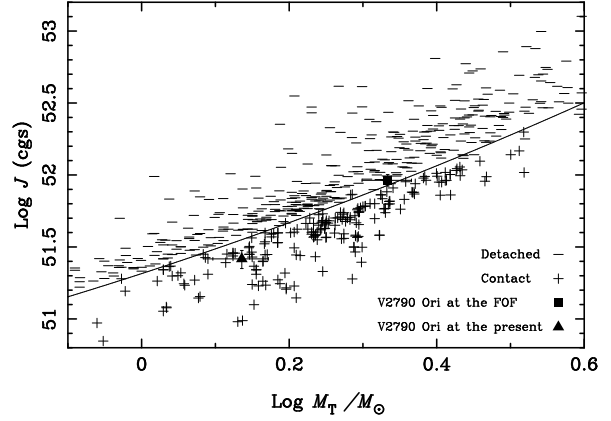

Fig. 6 Locations of V2790 Ori at the FOF (*filled square*) and the present time (*filled triangle*) on the $\log J_\mathrm{o} - \log M_\mathrm{T}$ diagram. The samples representing detached (Eker et al. 2006; Lee 2015; Yildiz & Doğan 2013) and contact (Eker et al. 2006; Ibanoğlu et al. 2006) are separated by the quadratic border line (Eker et al. 2006).

angular momentum at the FOF, J_FOF, can be calculated from Equation (9). According to a mass transfer process starting at the FOF and the lifetime in the detached phase for W-type typically being negligibly short (Yıldız 2014), we assumed that masses of both components were not much different from their initial values. Thus, for the beginning of the semi-detached phase, initial mass parameters from Table 5 were implemented in calculating J_FOF, while the orbital period and semimajor axis at the FOF were computed using Equations (10)–(11) (Yıldız 2014)

$$P_\mathrm{FOF} = 0.1159 \sqrt{\frac{a_\mathrm{FOF}^3}{M_\mathrm{Pi} + M_\mathrm{Si}}}, \qquad (10)$$

$$a_\mathrm{FOF} = \frac{0.6 q_\mathrm{i}^{2/3} + \ln(1 + q_\mathrm{i}^{1/3})}{0.49 q_\mathrm{i}^{2/3}} R_\mathrm{TAMS}, \qquad (11)$$

where P_FOF and a_FOF are the orbital period and semimajor axis at the FOF, respectively. R_TAMS is the Roche lobe radius filled by the massive component that evolved to reach TAMS. P_FOF, a_FOF and J_FOF are computed to be 1.083 ± 0.049 d, $5.731 \pm 0.090\,R_\odot$ and $9.39(\pm 0.73) \times 10^{51}$ cgs respectively. These results demonstrate that the angular momentum has decreased from 9.39×10^{51} cgs at the FOF to 2.62×10^{51} cgs at the present time, concurrently with a mass lost by the system of $0.789\,M_\odot$ as depicted in Figure 6. Consequently, the orbital period and semimajor axis have reduced from 1.083 d and $5.731\,R_\odot$ to 0.2878420 d and $2.036\,R_\odot$, respectively.

Initially, the binary V2790 Ori in the detached phase consisted of two main sequence stars. The more massive

component (the progenitor of the secondary component) has evolved to TAMS, leading to the resulting oversized envelope. In combination with AML, the Roche surface was filled by the evolved secondary component, causing mass transfer to begin. From the FOF until the present time, the orbit has been reduced by AML and mass loss.

6 CONCLUSIONS

In summary, the BVR_C observations were carried out at the Thai National Observatory, during three nights in 2015. The photometric data covered five eclipse timings. The $(O - C)$ curve shows an orbital period increase at a rate of $dP/dt = 1.03 \times 10^{-7} \, \text{d} \, \text{yr}^{-1}$. The observed light curves were fitted with the W-D method to provide fundamental parameters. It is found that V2790 Ori is a contact system with a mass ratio of $q = 2.932$. The estimated masses of the components are calculated to be $M_P = 1.020 \pm 0.112 \, M_\odot$ and $M_S = 0.348 \pm 0.038 \, M_\odot$ for the primary and secondary, respectively. With an orbital period increase, there could be mass transfer from the less massive secondary to the more massive primary with a rate of $6.31 \times 10^{-8} \, M_\odot \, \text{yr}^{-1}$.

Locations of V2790 Ori's components on the $\log M - \log L$ and $\log M - \log R$ diagrams confirm that the secondary has evolved to be overluminous and oversized, causing the envelope to fill its Roche surface, while the primary is still a main sequence star. Its mass and angular momentum have been lost continuously throughout its evolution from the detached phase to the contact phase. From the detached phase until the present time, there could be mass lost by the secondary of $1.188 \, M_\odot$, i.e., mass of $0.789 \, M_\odot$ lost by the system and mass of $0.399 \, M_\odot$ transferred to the primary. Also, 72.2% of the angular momentum has been lost from J_{FOF} since the FOF stage to the present time, yielding a smaller orbit.

References

Ammons, S. M., Robinson, S. E., Strader, J., et al. 2006, ApJ, 638, 1004

Chen, M., Xiang, F.-Y., Yu, Y.-X., & Xiao, T.-Y. 2015, RAA (Research in Astronomy and Astrophysics), 15, 275

Christopoulou, P.-E., & Papageorgiou, A. 2013, AJ, 146, 157

Demircan, O., Eker, Z., Karataş, Y., & Bilir, S. 2006, MNRAS, 366, 1511

Diethelm, R. 2011, Information Bulletin on Variable Stars, 5960

Diethelm, R. 2012, Information Bulletin on Variable Stars, 6011

Eker, Z., Demircan, O., Bilir, S., & Karataş, Y. 2006, MNRAS, 373, 1483

Eker, Z., Demircan, O., & Bilir, S. 2008, MNRAS, 386, 1756

Gazeas, K. D. 2009, Communications in Asteroseismology, 159, 129

Gazeas, K., & Stępień, K. 2008, MNRAS, 390, 1577

Guo, D. F., Li, K., Hu, S. M., & Chen, X. 2018, PASP, 130, 064201

Hubscher, J. 2013, Information Bulletin on Variable Stars, 6084

Hurley, J. R., Tout, C. A., & Pols, O. R. 2002, MNRAS, 329, 897

Ibanoğlu, C., Soydugan, F., Soydugan, E., & Dervişoğlu, A. 2006, MNRAS, 373, 435

Iben, Jr., I., & Tutukov, A. V. 1984, ApJS, 54, 335

Jiang, D., Han, Z., & Li, L. 2014, MNRAS, 438, 859

Jurýsek, J., Hoňková, K., Šmelcer, L., et al. 2017, Open European Journal on Variable Stars, 179, 1

Lee, C.-H. 2015, MNRAS, 454, 2946

Lee, J. W., Lee, C.-U., Kim, S.-L., Kim, H.-I., & Park, J.-H. 2011, PASP, 123, 34

Li, K., Hu, S.-M., Guo, D.-F., et al. 2015, AJ, 149, 120

Li, K., Hu, S.-M., Jiang, Y.-G., Chen, X., & Ren, D.-Y. 2014, New Astron., 30, 64

Li, K., Xia, Q.-Q., Hu, S.-M., Guo, D.-F., & Chen, X. 2018, PASP, 130, 074201

McDonald, I., Zijlstra, A. A., & Watson, R. A. 2017, MNRAS, 471, 770

Michaels, E. J. 2016, Journal of the American Association of Variable Star Observers (JAAVSO), 44, 30

Mochnacki, S. W. 1981, ApJ, 245, 650

Nagai, K. 2012, Variable Star Bull. 53, 1

Nagai, K. 2013, Variable Star Bull. 55, 1

Nagai, K. 2014, Variable Star Bull. 56, 1

Nagai, K. 2016, Variable Star Bull. 61, 1

Nelson, R. H. 2011, Information Bulletin on Variable Stars, 5966

Nelson, R. H. 2012, Information Bulletin on Variable Stars, 6018

Oelkers, R. J., Rodriguez, J. E., Stassun, K. G., et al. 2018, AJ, 155, 39

Ostadnezhad, S., Delband, M., & Hasanzadeh, A. 2014, New Astron., 31, 14

Otero, S. A., Wils, P., & Dubovsky, P. A. 2004, Information Bulletin on Variable Stars, 5570

Pribulla, T. 1998, Contributions of the Astronomical Observatory Skalnate Pleso, 28, 101

Qian, S. 2003, MNRAS, 342, 1260

Qian, S.-B., Yuan, J.-Z., Xiang, F.-Y., et al. 2007, AJ, 134, 1769

Rucinski, S. M. 1986, in IAU Symposium, 118, Instrumentation and Research Programmes for Small Telescopes, eds. J. B. Hearnshaw, & P. L. Cottrell, 159

Sarotsakulchai, T., Qian, S.-B., Soonthornthum, B., et al. 2019, PASJ, 71, 34

Singh, M., & Chaubey, U. S. 1986, Ap&SS, 124, 389

Stępień, K., & Gazeas, K. 2012, Acta Astronomica, 62, 153

Tutukov, A. V., Dremova, G. N., & Svechnikov, M. A. 2004, Astronomy Reports, 48, 219

Vilhu, O. 1981, Ap&SS, 78, 401

Wilson, R. E. 1979, ApJ, 234, 1054

Wilson, R. E. 2012, AJ, 144, 73

Wilson, R. E., & Devinney, E. J. 1971, ApJ, 166, 605

Wilson, R. E., Van Hamme, W., & Terrell, D. 2010, ApJ, 723, 1469

Yakut, K., & Eggleton, P. P. 2005, ApJ, 629, 1055

Yıldız, M. 2014, MNRAS, 437, 185

Yildiz, M., & Doğan, T. 2013, MNRAS, 430, 2029

Yu, Y.-X., Xiang, F.-Y., & Hu, K. 2016, PASP, 128, 044202

Zhang, X. B., Deng, L., & Lu, P. 2009, AJ, 138, 680